Deglacial temperature history of West Antarctica

Kurt M. Cuffey[a,1], Gary D. Clow[b], Eric J. Steig[c], Christo Buizert[d], T. J. Fudge[c], Michelle Koutnik[c], Edwin D. Waddington[c], Richard B. Alley[e], and Jeffrey P. Severinghaus[f]

[a]Department of Geography, University of California, Berkeley, CA 94720; [b]Geosciences and Environmental Change Science Center, United States Geological Survey, Lakewood, CO 80225; [c]Department of Earth and Space Sciences, University of Washington, Seattle, WA 98195; [d]College of Earth, Ocean, and Atmospheric Sciences, Oregon State University, Corvallis, OR 97331; [e]Department of Geosciences, The Pennsylvania State University, University Park, PA 16802; and [f]Scripps Institution of Oceanography, University of California, San Diego, La Jolla, CA 92093

Edited by Mark H. Thiemens, University of California, San Diego, La Jolla, CA, and approved October 19, 2016 (received for review June 6, 2016)

The most recent glacial to interglacial transition constitutes a remarkable natural experiment for learning how Earth's climate responds to various forcings, including a rise in atmospheric CO_2. This transition has left a direct thermal remnant in the polar ice sheets, where the exceptional purity and continual accumulation of ice permit analyses not possible in other settings. For Antarctica, the deglacial warming has previously been constrained only by the water isotopic composition in ice cores, without an absolute thermometric assessment of the isotopes' sensitivity to temperature. To overcome this limitation, we measured temperatures in a deep borehole and analyzed them together with ice-core data to reconstruct the surface temperature history of West Antarctica. The deglacial warming was 11.3 ± 1.8 °C, approximately two to three times the global average, in agreement with theoretical expectations for Antarctic amplification of planetary temperature changes. Consistent with evidence from glacier retreat in Southern Hemisphere mountain ranges, the Antarctic warming was mostly completed by 15 kyBP, several millennia earlier than in the Northern Hemisphere. These results constrain the role of variable oceanic heat transport between hemispheres during deglaciation and quantitatively bound the direct influence of global climate forcings on Antarctic temperature. Although climate models perform well on average in this context, some recent syntheses of deglacial climate history have underestimated Antarctic warming and the models with lowest sensitivity can be discounted.

climate | paleoclimate | Antarctica | glaciology | temperature

From the Last Glacial Maximum (LGM) around 21 ka to the middle of the Holocene, increased greenhouse gas concentrations and reduced reflectivities of the surface and atmosphere directly increased the uptake of energy to Earth's climate system by about $7 W \cdot m^{-2}$ (1–3) and warmed the surface by 3–6 °C on average (4–7). Although contributing little to this global average because of the comparatively small area involved, the warming in polar regions holds particular interest. In addition to driving changes of ice sheets, permafrost, and hydrology and modulating oceanic and atmospheric circulations, polar warming partly controlled both the evolution of surface reflectivity and the transfer of carbon dioxide from ocean to atmosphere and hence the climate forcing itself. Further, reconstructions of polar warming during deglaciation permit quantification of one key prediction of climate theory—that feedback processes amplify temperature changes in polar regions relative to the global average (4, 8, 9), a phenomenon referred to as polar amplification. Arctic data reveal a warming three to four times the global average based on a wide variety of indicators (6), including combined analyses of ice-core data and borehole temperatures (10, 11). Limited available constraints suggest a smaller but still amplified Antarctic warming, roughly 1.5 to 2.5 times greater than the global average (6, 12). This Antarctic estimate, however, derives from the isotopic composition of ice measured in cores. The scaling between ice isotopic composition and temperature depends on a great many factors (section 15.5 in ref. 13), such as the seasonal timing of snowfall and rate-dependent fractionations in clouds, that remain poorly known and are expected to vary with time. Moreover, the low accumulation rates at East Antarctic core sites have precluded convincing quantifications of the isotopic thermometers using independent information from borehole temperatures, the most direct legacy of past climate. One Antarctic study used such information (14), but the small accumulation rate at the site meant that diffusive heat transport greatly dominated advection, rendering the method imprecise.

Here we present a reconstruction of West Antarctic temperature history from the site of the West Antarctic Ice Sheet Divide ice core (WDC) (15, 16). This site is uniquely suitable for analyses using borehole temperatures, given the combination of thick ice and high snow accumulation rate, together with the wealth of information provided by the 68-ky core record. Elsewhere, similarly favorable conditions prevail only in central Greenland (10).

Reconstruction

We measured temperatures in the 3.4-km-deep WDC borehole (*Materials and Methods*). The temperature profile reveals a direct thermal remnant of the deglacial transition and subsequent Holocene temperature changes (Fig. 1).

Because of diffusive smoothing, borehole temperatures contain information about only long-term averages of climatic temperatures (*SI Reconstruction Strategy*). Our analysis therefore incorporates two additional sources of thermometric information from the core: the deuterium isotopic composition of ice (δD) and the nitrogen isotopic composition of trapped gas (δ^{15}N) (*SI Ice-Isotopic Data* and *SI Nitrogen-Isotopic Data* and

Significance

The magnitude and timing of Antarctic temperature change through the last deglaciation reveal key aspects of Earth's climate system. Prior attempts to reconstruct this history relied on isotopic indicators without absolute calibration. To overcome this limitation, we combined isotopic data with measurements of in situ temperatures along a 3.4-km-deep borehole. Deglacial warming in Antarctica was two to three times larger than the contemporaneous global temperature change, quantifying the extent to which feedback processes amplify global changes in polar regions, a key prediction of climate models. Warming progressed earlier in Antarctica than in the Northern Hemisphere but coincident with glacier recession in southern mountain ranges, a manifestation of changing oceanic heat transport, insolation, and atmospheric CO_2 that can further test models.

Author contributions: K.M.C. and C.B. designed research; K.M.C., G.D.C., E.J.S., C.B., T.J.F., M.K., E.D.W., R.B.A., and J.P.S. performed research; K.M.C., G.D.C., E.J.S., C.B., T.J.F., M.K., and E.D.W. analyzed data; and K.M.C. wrote the paper.

The authors declare no conflict of interest.

This article is a PNAS Direct Submission.

Freely available online through the PNAS open access option.

[1]To whom correspondence should be addressed. Email: kcuffey@berkeley.edu.

This article contains supporting information online at www.pnas.org/lookup/suppl/doi:10.1073/pnas.1609132113/-/DCSupplemental.

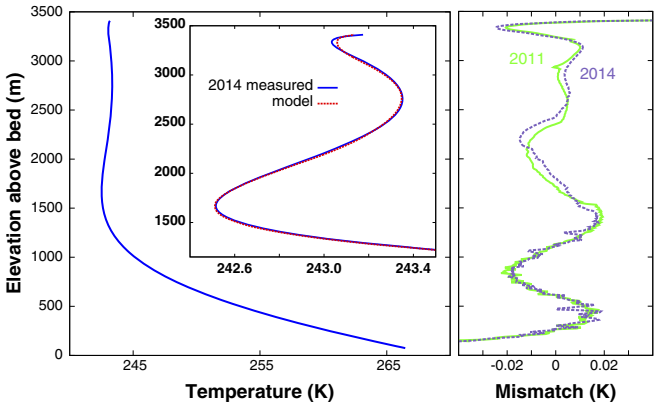

Fig. 1. Observed and modeled temperatures in the WAIS Divide borehole. (*Left*) Ice temperature profile observed in 2014. At this scale the model and measurements are indistinguishable, as are the profiles measured in 2011 and 2014. *Left Inset* expands the upper portion and compares the model to the 2014 observation. The cold region centered around 1,700 m is a remnant of the last glacial climate. (*Right*) Difference between observed temperatures and optimal models (model minus observed), for both the 2011 and 2014 measurements.

Fig. S1). Although not perfect thermometers, isotopic data provide a constraint based on temperature-dependent physical processes, and their use avoids a priori assumptions about climate variability that are otherwise required for interpreting borehole temperatures. The temperature (T) dependence of δD arises from atmospheric distillation processes (17) and, despite potential complexities, is usually treated as a linear relationship: $\delta = \gamma\, T + \beta$. Due to gravitational settling of heavy gases, δ^{15}N measures the thickness of firn (18, 19), the 50- to 120-m-deep porous layer of consolidated snow that blankets the ice-sheet surface. Firn densification proceeds at a rate dependent on both temperature and loading, so firn thickness depends on both temperature and accumulation rate (20, 21). Higher temperatures and slower accumulation both produce thinner firn, reducing δ^{15}N.

To determine the surface temperature history $T_s\,(t)$, we optimized the match between temperatures measured in the borehole and those calculated with a numerical model of heat transfer driven by various $T_s\,(t)$ scenarios as a boundary condition (*Materials and Methods* and *SI Calculation of Temperatures vs. Depth*). To start, we filtered the deuterium ice-isotopic record (δD) to remove high-frequency variability. Using the time derivative of this filtered history ($\dot{\delta}$), we then optimized the temperature variation (relative to modern) given by

$$\Delta T_s\,(\delta) = \int_t \gamma^{-1}(t)\,\dot{\delta}(t)\,dt, \qquad [1]$$

where the coefficient $\gamma\,(t)$ takes three values (Table S1), one for each of the three major periods of isotopic change (deglacial, early to mid-Holocene, and late Holocene). Fig. 2*A* shows the result. This calibrated $\Delta T_s\,(\delta)$ is then used without further adjustments in subsequent optimizations of

$$T_s\,(t) = T_o + \Delta T_s(\delta) + \sum_{i=1}^{3} c_i \cdot g_i(t) + \omega(t) \cdot \Delta T_{\mathrm{N}}(t) \qquad [2]$$

in which the free parameters are three coefficients c_i and a constant T_o, the modern temperature. This relation introduces three basis functions $g_i\,(t)$, with ranges $\in (0, 1)$ that reflect the broadest pattern of variations seen in the observed temperature–depth profile. They allow for adjustments to reconstructed average temperatures of the late glacial period, early Holocene, and mid- to late Holocene (*SI Basis Functions* and Fig. S2). Magnitudes are within $\pm 0.5\,^{\circ}$C in the final reconstruction.

To incorporate δ^{15}N data, the temperature history can be adjusted further by an amount ΔT_{N} determined by densification physics to reconcile the accumulation rate histories derived two independent ways (*Materials and Methods* and *SI Firn Thickness Model and Use of Nitrogen Isotope Data*): one from $T_s(t)$ and δ^{15}N using a model for the evolving firn density and thickness and a second one from the ice core's observed annual layer thicknesses, corrected for strain using glaciological parameters determined in the optimization of Eq. **2**. The multiplier $\omega(t)$ ranges between 0 and 1, allowing us to control the relative importance of ice and gas isotopic records. It safeguards against possible problems with the nitrogen isotope method; the accuracy of ΔT_{N} as a thermometer is not well established, especially given imperfections of firn densification models and irregularities of the gas-trapping process at the firn base. We examined reconstructions with various ω values and used borehole temperatures to identify the range of admissible scenarios (*SI Calculation of Limits and Tolerance*).

Our final reconstruction (Fig. 2) uses $\omega > 0.5$ for all but the late Holocene (*Materials and Methods* and *SI Firn Thick-*

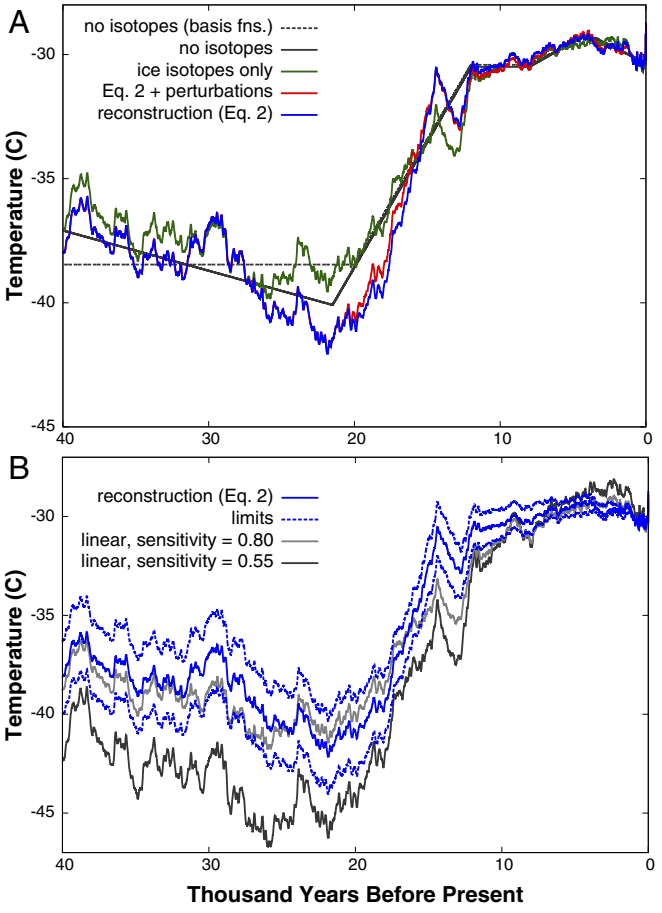

Fig. 2. Optimal West Antarctic Divide surface temperature reconstructions. The blue curve, our optimal reconstruction using Eq. **2** without random perturbations, is identical in *A* and *B*. (*A*) Eq. **1** (green), Eq. **2** (blue), and Eq. **2** plus random perturbations (red). Also shown are calibrated basis functions without isotopes (dashed black) and the same with prescribed cooling before 21 ka (solid black). (*B*) Our final reconstruction [Eq. **2** (blue)] and model-dependent $\pm 2\sigma$ limits as defined in *SI Calculation of Limits and Tolerance* (dashed blue), together with linearly scaled ice-isotope curves with sensitivities γ_{18} = 0.55‰ and 0.80‰ $^{\circ}$C^{-1} (gray).

ness Model and Use of Nitrogen Isotope Data, *The Coefficient* ω) and gives a match between model and observed temperature profiles with a root-mean-square error of 1.47 cK (Table S2). This is an excellent match considering the total range of the temperature profile (Fig. 1), but still larger than the 0.8-cK tolerance defined by uncertainties in the measurement and in glaciological variables (*SI Calculation of Limits and Tolerance*). To assess how much of the remaining mismatch could be eliminated without altering the broad patterns implied by δD and δ^{15}N, we introduced a random perturbation term to Eq. **2** before optimization (*SI Reconstruction Strategy*) and tested various scenarios. The best one reduced the rms error to 1.11 cK. Fig. 1 illustrates its match between model and observed temperature–depth profiles. This improvement is not large enough to negate the model without perturbations and regardless is achieved without any significant changes in the reconstructed temperature (Fig. 2*A*). In contrast, the optimized Eq. **1** using ice isotopes alone can be firmly rejected, as can optimized basis functions without isotopes (Fig. 2*A* and Table S2). Table S2 summarizes metrics of model performance for all stages of the analysis. We note that using $\omega = 1$ instead of $\omega = 0$ in Eq. **2** significantly improves model performance, providing evidence that the firn-thickness proxy serves as a thermometer despite potential complexities in the controls on firn structure and gas transport.

The true total uncertainty of reconstructed temperatures is difficult to define, given that borehole temperatures preserve only long-term averages of the climatic forcing and given the possible nonthermal influences on the isotopic proxies providing higher-frequency information. Within the context of our reconstruction strategy, however, we can define limits by accounting for sources of uncertainty in input variables and arbitrary model choices (Table S4). The limits (Fig. 2*B*) are the quadrature sum of 2σ uncertainties arising from model parameters and methodological choices, as summarized in *Materials and Methods* and *SI Calculation of Limits and Tolerance*.

Perspective on the utility of our reconstruction can be gained by comparison with temperature histories derived from the traditional method of treating temperatures as a single linear function of ice-isotopic data ($\delta = \gamma\, T + \beta$, with constant γ dependent on whether δ refers to deuterium (D) or oxygen-18 content, such that $\gamma_{\mathrm{D}} = 8\,\gamma_{18}$). Estimates of γ from studies of temporal and spatial covariation of δ and T in Antarctica range from $\gamma_{18} \approx 0.4‰\,^{\circ}\mathrm{C}^{-1}$ to $1.0‰\,^{\circ}\mathrm{C}^{-1}$ (22, 23), corresponding to approximately $\pm 5.5\,^{\circ}\mathrm{C}$ of uncertainty in the LGM temperature at West Antarctic Ice Sheet Divide, three times the uncertainty of our reconstruction. Estimates of γ from temporal covariations, presumably the most relevant for climate reconstruction, average $\gamma_{18} \approx 0.55‰\,^{\circ}\mathrm{C}^{-1}$ (24), whereas the continent-wide spatial covariation gives $\gamma_{18} \approx 0.8\,‰\,^{\circ}\mathrm{C}^{-1}$ (22, 25). Fig. 2*B* plots these two cases in comparison with our reconstruction. The LGM temperature given by the temporal sensitivity is too cold, whereas, surprisingly, the spatial one matches our reconstruction well. Both, however, are too cold in the second half of the deglaciation, 15–9 ka. That the comparative warmth of this interval emerges strongly from the borehole temperature data is apparent from both the range of our optimal reconstruction (Fig. 2*B*) and the shape of the simple nonisotopic models (Fig. 2*A*).

Discussion

Our surface temperature reconstruction (Fig. 2*B*) indicates that the surface in central West Antarctica was colder during the LGM (average from 20 ka to 23 ka) than in the late Holocene by $11.3 \pm 1.8\,^{\circ}\mathrm{C}$ (2σ) (Table S3), whereas the net warming from the LGM to the middle Holocene thermal maximum (3–6 ka at this site) was perhaps as large as $13.7\,^{\circ}\mathrm{C}$. Cited estimates for the deglacial warming at locations in East Antarctica are smaller, from $7\,^{\circ}\mathrm{C}$ to $9.3\,^{\circ}\mathrm{C}$ at the ice-core sites Vostok, Dronning Maud Land, Talos Dome, Dome F, and Dome C (6, 12, 26). It is possible that there exists a real regional difference from West Antarctica, where the climate is more strongly influenced by the proximal ocean (24, 27), but these values all derive from assumptions about the sensitivity of ice isotopes to climatic temperature, a method known to be inaccurate in Greenland (10, 28).

Influence of Elevation and Thickness Changes. Our reconstruction is of temperature at the ice-sheet surface. Some aspects of the deglacial and Holocene temperature variations likely arise from changes of surface elevation via the atmospheric lapse rate. Further, the history of ice thickness influences our reconstructed surface temperature directly; thinning is associated with increased vertical ice velocity, which would shift reconstructed LGM temperatures to warmer values (*SI Influence of Elevation and Thickness Changes on Interpretation of Reconstructed Temperatures* and Fig. S3). A plausible upper-limit case of 300 m thinning at WAIS Divide in the last 15 ky (29–31), preceded by thickening due to the known deglacial accumulation increase, warms our reconstructed LGM surface temperature by $\sim 0.5\,^{\circ}\mathrm{C}$. For this reason, the limits of our LGM temperatures shown in Fig. 2*B* have been expanded by this magnitude. Including the lapse rate effect from such a thinning (adjusted for isostasy) would imply a constant-elevation temperature change from LGM to Holocene of $10.2 \pm 1.4\,^{\circ}\mathrm{C}$ (*SI Influence of Elevation and Thickness Changes on Interpretation of Reconstructed Temperatures*), which overlaps the range of surface temperatures shown in Fig. 2*B*. Glaciological reasoning, ice-sheet model simulations, and geological constraints all suggest that smaller elevation changes are more likely, indicating that a smaller or possibly even negligible correction between surface temperature and constant-elevation temperature is more appropriate.

Climatic Implications. Climate models predict that global temperature changes are amplified in the polar regions by feedback processes involving atmospheric moisture transport, soil moisture, heat exchange through sea ice, and the dependence of longwave emissions and lapse rate on surface temperature, and by factors controlling surface albedo: sea ice, ice sheets, snow, and vegetation (4, 8, 9, 32). All of these operate in the Arctic, but the much smaller land area reduces or eliminates some of them in the Antarctic. Averaging results from various climate model simulations of the LGM (21 ka) gives a global average cooling relative to late Holocene of $\sim 4.4\,^{\circ}\mathrm{C}$ compared with an Antarctic (south of $80\,^{\circ}\mathrm{S}$) mean of $11 \pm 4\,^{\circ}\mathrm{C}$ (4). Our result for West Antarctica lies in the middle of the models' rather broad range and implies that Antarctic amplification through the deglacial climate transition was a factor of 2–3. A smaller contrast is expected in comparisons focused on mid-latitude sites. In the interval 18–15 ka, we find that West Antarctica warmed by about $7\,^{\circ}\mathrm{C}$, compared with about $4\,^{\circ}\mathrm{C}$ indicated by glacier retreat in New Zealand (33).

Fig. 3*A* illustrates how our West Antarctic history compares to estimated global-averaged temperature based on proxy records interpreted in a model context (6, 34). Some estimates of the global temperature depression at LGM are as small as $3.6\,^{\circ}\mathrm{C}$, whereas others are as large as $5.8\,^{\circ}\mathrm{C}$ (6, 7), and the two global curves in Fig. 3*A* are scaled to match this range. Note that the only proxies contributing to the estimated global temperature history (6) from latitudes poleward of $55^{\circ}\mathrm{S}$ are the isotopes from the four East Antarctic ice cores. Our results imply this might be a source of bias, most likely an underestimate of temperature change at high latitudes.

A recent synthesis of climate sensitivities estimated from paleoclimate data (35) concluded that a doubling of atmospheric CO_2 would increase global temperature by 2.2–4.8 °C (68% probability), values similar to or slightly higher than ones derived

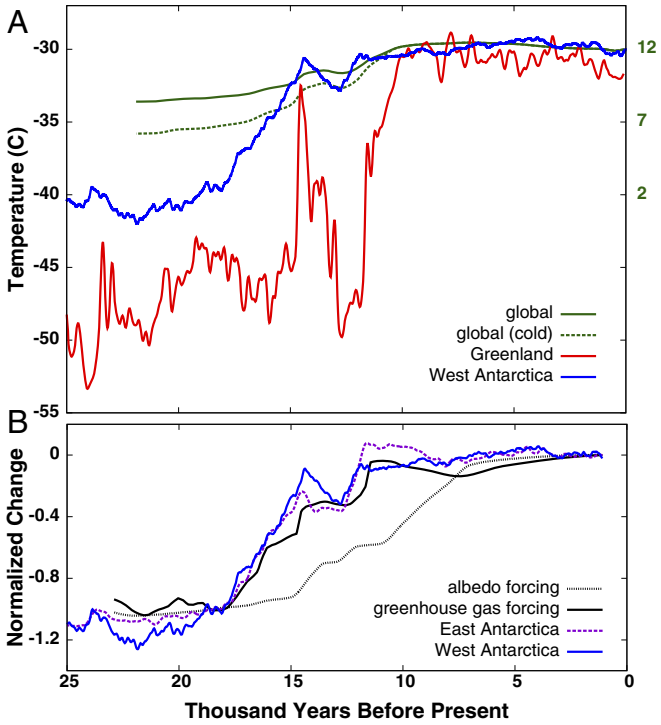

Fig. 3. Comparisons of temperature histories and forcings. (*A*) This study's optimal West Antarctic Divide surface temperature history (blue and left axis) from Eq. **2**, central Greenland temperature history (red and left axis) from ref. 10, and global-average temperature from studies of the deglacial period (6) and the Holocene (34) with an LGM temperature 3.6 °C below modern (solid green and right axis) and scaled at ages greater than 11 ka to reach the colder LGM (−5.8 °C) implied by ref. 7 (dashed green and right axis). The best-constrained studies yield an LGM temperature between these (5). (*B*) Various histories of forcings and temperatures (to facilitate comparisons of relative timing, the histories are all scaled to range from zero to unity between 18.5 ka and 1 ka, times of nearly identical annually integrated insolation at 70 °S): optimal West Antarctic Divide surface temperature (solid blue), average of East Antarctic ice cores (26) (dashed purple), methane and carbon dioxide greenhouse gas climate forcing (46) (solid black), and ice-sheet area albedo forcing calculated as sea-level change raised to the power 0.8 according to the average relationship between ice-sheet area and volume (section 8.10.3 in ref. 13) (dotted black).

by other techniques. Those paleoclimate studies using Antarctic data have likely underestimated the temperature change in response to the well-constrained change in CO_2 and thus underestimated climate sensitivity. In particular, the analysis producing the lowest estimated sensitivity in the compilation (36, 37) (a bit larger than 2.2 °C) predicted an Antarctic LGM cooling smaller than even estimates from the East Antarctic isotopic proxies. Our reconstruction affirms that this is an underprediction. Antarctica accounts for a small fraction of global area and hence does not contribute much directly to climate sensitivity estimates, but the discrepancy may indicate too-weak feedbacks in some of the models used to assimilate proxy data.

A noteworthy aspect of our reconstruction is that by 15 ka, the millennial-averaged temperature had risen to within ∼2.5 °C of its late Holocene value (Fig. 2). The fraction of deglacial warming accomplished by this time was most likely 0.77±0.05 (Table S3). Such early warming of West Antarctica is consistent with inferences from retreat of glaciers in Southern Hemisphere mountain ranges. Extensive retreat occurred between 18 ka and 14.5 ka in Patagonia (38), with the Patagonian ice cap attaining near-present dimensions by 15.5 ka (39). Glaciers in the New Zealand Alps largely completed their major retreat by 15.7 ka (40). Thus, our temperature reconstruction and glacial geologic proxies both confirm a significant inference from isotopic records (6, 26, 41) that the high latitudes of the Southern Hemisphere experienced much of their warming millennia before the Arctic. At 15 ka Greenland had warmed by perhaps 5 °C (Fig. 3*A*), or less than 30% of the deglacial total (10), and did not maintain interglacial temperatures until around 11 ka, four millennia later than in West Antarctica.

Global climate evolution of the last deglaciation is regarded as the superposition of two modes (41): a global warming following radiative forcing and an interhemispheric redistribution of heat following variations in cross-equatorial heat transport by the Atlantic Meridional Overturning Circulation. Reduced Atlantic heat transport between 19 ka and 14.7 ka (Heinrich Stadial 1) cooled Greenland and contributed to the early Antarctic warming. Climate model experiments suggest that this contribution amounted to no more than a few degrees (42), however, and other factors such as increased insolation and associated sea ice feedbacks were probably important (15, 43). How these processes combined to produce the comparatively large inferred warming remains uncertain and offers a potentially illuminating target for further model studies.

In the period of early warming, 18.5–15 ka, increasing annually integrated insolation and reduced northward oceanic heat transport account for a climate forcing of 1 to a few watts per meter^2 specific to the Southern Hemisphere (*SI Climate Forcings During Deglaciation*). This can be compared with the global forcings governing the difference between planetary temperatures of the LGM and Holocene. Taken together, decreasing ice-sheet extent (hence reduced albedo) and increasing greenhouse gas concentrations (CO_2 and CH_4) account for about 90% of the direct global-averaged climate forcing, with respective magnitudes of ∼2.9 W·m^2 and 2.2 W·m^{-2} (2). Fig. 3*B* plots histories of these two forcings. Antarctic warming leads the greenhouse gas forcing through the deglaciation, and the fractional increases (Fig. 3*B*) put an upper limit on the contribution of the gases to Antarctic warming between 18.5 ka and 15 ka of ∼65%. The magnitude of the gas forcing by 15 ka was ∼1 W·m^{-2}, equal to or somewhat smaller than the forcing from combined insolation and reduced ocean transport. Given this similarity, the observation that CO_2 could account for roughly half of the warming is consistent with normative estimates of its climatic impact.

Fig. 3*B* also shows strong similarities between our West Antarctic temperature history and a composite of the ice-isotopic records from interior East Antarctica (26), although the latter covaries yet more closely with the greenhouse forcing. In the Holocene, a maximum at around 4 ka appears in both parts of the continent, with a West Antarctic magnitude of 0.6–1.2 °C warmer than the last millennium (0–1 ka). Differences at other times might record changes of elevation, sea ice, or other factors. The West Antarctic warming just before 18 ka, attributed previously to insolation driving Southern Ocean warming and sea ice retreat to which East Antarctic isotopes are less sensitive (15), appears in Chile as glacier advance and in New Zealand as glacier retreat punctuated by readvances that left moraines (33, 44). These glaciers are thought to respond to Southern Ocean temperatures as well (45).

Conclusion

The temperature reconstruction reported here provides information about the thermal state of firn and ice through time at the West Antarctic Divide site, an essential input to studies of the depth–age relationship, interhemispheric climate phasing, CO_2 history, and covariation of temperature with accumulation (16, 47, 48). Of greatest immediate interest, however, is our demonstration that the global deglacial temperature change was amplified by a factor of 2–3 in the Antarctic, that Antarctic warming was largely achieved by 15 ka in coherence with records from Southern Hemisphere mountain ranges, and that climate

models of the deglaciation perform well on average, but that the ones with lowest sensitivity can be discounted. The early warming of the Southern Hemisphere, which our study helps to quantify, arose from combined effects of reduced northward oceanic heat transport, increased insolation, and increasing atmospheric CO_2. Quantitative simulation of this phenomenon could provide an illuminating challenge for model studies.

Materials and Methods

Calculation of Temperatures as a Function of Depth. We used the control-volume method (49) to solve the one-dimensional time-dependent energy balance equation accounting for conduction, advection, and sources (*SI Calculation of Temperatures vs. Depth*).

Optimization. Singular value decomposition was used to find parameter values that minimized the squared mismatch of modeled and measured temperatures. Every such optimization involved free parameters related to surface temperature variations plus three additional free parameters: the modern mean surface temperature, the present ice thickness (known to be in the range 3,450–3,470 m), and the rate of basal melt. The latter accounts for the geothermal heat flux, which is not an independent parameter. The number of simultaneous free parameters in all optimizations (Eqs. **1** and **2**) remains constant (six).

Measurement of Borehole Temperatures. Temperatures in the fluid-filled WDC borehole were logged during December 2011 and again during December 2014, using the US Geological Survey Polar Temperature Logging System (PTLS) (50, 51) (*SI Measurement of Borehole Temperatures*). Combined uncertainties in assessing temperatures in the surrounding ice are ~5.3 mK for the fluid-filled portion of the borehole (depths >96 m). Above 96 m we used the temperature profile previously measured in a neighboring air-filled hole (52), shifted uniformly to match the values determined by the more accurate PTLS measurements.

Ice-Core Data. Measurements of δD of ice and δ^{15}N of trapped N_2 were by laser spectroscopy and mass spectrometry, respectively (15, 47) (*SI Ice-Isotopic Data* and *SI Nitrogen-Isotopic Data*). The age–depth relation and annual layer thicknesses were determined by identifying and counting annual layers back to ~31 ka and by cross-correlations of gas records prior to this time (16, 47, 53) (*SI Age–Depth Relation and Layer Thicknesses*).

Firn Thickness Model and Use of Nitrogen Isotope Data. *SI Firn Thickness Model and Use of Nitrogen Isotope Data* provides more information.

Calculation of $\delta^{15}N(t)$. Given simultaneous histories of accumulation rate ($\dot{b}(t)$) and $T_s(t)$, we calculated firn density profiles using an empirical model (20), recast to use overburden load as a driving variable as in refs. 28 and 47. The density profile, in turn, is used to calculate δ^{15}N(t) of gas at the depth of trapping, accounting for gravitational settling, thermal fractionation, and near-surface convective mixing with the atmosphere. The calculated δ^{15}N for current climate matches the observed modern value.

Calculation of $\Delta T_N(t)$. We first calculated δ^{15}N(t) using an initial $\dot{b}(t)$ derived from observed ice-core layer thicknesses and the strain model associated with an initial optimized $T_s(t)$. Comparison with measured δ^{15}N(t) then defined an adjustment to $\dot{b}(t)$. This process was iterated until measured and modeled δ^{15} N(t) agreed as well as possible (Fig. S1), following the method described in refs. 28 and 47. The temperature-history correction $\Delta T_N(t)$ was then calculated as a function of the ratio of the adjusted $\dot{b}(t)$ to the initial $\dot{b}(t)$. This function describes the coupled dependence of δ^{15}N on temperature and accumulation rate according to firn density models and the barometric equation and has been calibrated against modern-day observations and various sites. The entire process was iterated several times. Fig. S1 illustrates the close match between the optimized model's two histories of accumulation rate, one estimated from ice strain and the other from reconstructed temperatures via δ^{15}N. We also repeated analyses with two alternative firn densification models (21, 54).

The coefficient ω in Eq. 2. As a function of age our optimized model uses $\omega = 0$ for <3 ka, $\omega = 1$ for 3.5–12 ka, and $\omega \approx 0.5$ for >15 ka (see *SI Firn Thickness Model and Use of Nitrogen Isotope Data*, *The Coefficient ω* for explanation). Alternative variations of $\omega(t)$ are used in defining limits on the temperature history.

Calculation of $\pm 2\sigma$ Limits on Reconstructed Temperature. We perturbed uncertain input variables and recalculated optimal temperature histories. The most important variables proved to be the ice thickness history, depth–age scale, and thermal conductivity of ice (*SI Calculation of Limits and Tolerance*). In addition, we used such recalculations to assess the impact of altering choices about model strategy, including the shape and timing of basis functions and values of the coefficient ω, both in Eq. **2**. Finally, we assessed the uncertainty arising from upstream variations of flow and temperature by comparing results from our one-dimensional model with those from a 2D model. The limits shown in Fig. 2*B* derive from quadrature sums of all these effects.

Data Availability. All data are available online through the U.S. Antarctic Program Data Center (http://www.usap-data.org/).

ACKNOWLEDGMENTS. We are deeply indebted to many participants in the WDC project and especially thank K. Taylor, E. J. Brook, and J. W. C. White. The helpful comments of two anonymous referees are gratefully acknowledged. This work is funded through the US National Science Foundation Grants 0539232, 0537661 (to K.M.C.), 0537930, 1043092 (to E.J.S.), 1043518 (to C.B.), 0944199, 0944197, 0440666 (to E.D.W.), 0539578, 1043528, 1338832 (to R.B.A.), and 0538657 (to J.P.S.) and National Aeronautics and Space Administration Grant NNX12AB74G (to M.K.). We gratefully acknowledge additional support from the Martin Family Foundation (K.M.C.), the USGS Climate and Land Use Change Program (G.D.C.), and National Oceanic and Atmospheric Administration Climate and Global Change Fellowships (C.B.).

1. Hansen J, et al. (1984) Climate sensitivity: Analysis of feedback mechanisms. *Geophys Monogr* 29:130–163.
2. Hewitt CD, Mitchell JFB (1997) Radiative forcing and response of a GCM to ice age boundary conditions: Cloud feedback and climate sensitivity. *Clim Dynam* 13:821–834.
3. Claquin T, et al. (2003) Radiative forcing of climate by ice-age atmospheric dust. *Clim Dynam* 20:193–202.
4. Masson-Delmotte V, et al. (2013) Information from paleoclimate archives. *Climate Change 2013: The Physical Science Basis. Contribution of Working Group I to the Fifth Assessment Report of the Intergovernmental Panel on Climate Change*, eds Stocker TF, et al. (Cambridge University Press, New York), Chap 5, pp 383–464.
5. Annan JD, Hargreaves JC (2013) A new global reconstruction of temperature changes at the last glacial maximum. *Clim Past* 9:367–376.
6. Shakun JD, et al. (2012) Global warming preceded by increasing carbon dioxide concentrations during the last deglaciation. *Nature* 484:49–55.
7. von Deimling TS, Ganopolski A, Held S, Rahmstorf S (2006) How cold was the last glacial maximum? *Geophys Res Lett* 33:L14709.
8. Pithan F, Mauritsen T (2014) Arctic amplification dominated by temperature feedbacks in contemporary climate models. *Nat Geosci* 7:181–184.
9. Graversen RG, Langen PL, Mauritsen T (2014) Polar amplification in CCSM4: Contributions from the lapse rate and surface albedo feedbacks. *J Clim* 27:4433–4450.
10. Cuffey KM, et al. (1995) Large arctic temperature change at the Wisconsin-Holocene glacial transition. *Science* 270:455–458.
11. Dahl-Jensen D, et al. (1998) Past temperatures directly from the Greenland ice sheet. *Science* 282:268–271.
12. Masson-Delmotte V, et al. (2011) A comparison of the present and last interglacial periods in six Antarctic ice cores. *Clim Past* 7:397–423.
13. Cuffey K, Paterson W (2010) *The Physics of Glaciers* (Elsevier, Burlington, MA), 4th Ed.
14. Salamatin AN, et al. (1998) Ice core age dating and paleothermometer calibration based on isotope and temperature profiles from deep boreholes at Vostok Station (East Antarctica). *J Geophys Res* 103(D8):8963–8978.
15. WAIS Divide Project Members (2013) Onset of deglacial warming in West Antarctica driven by local orbital forcing. *Nature* 500:440–444.
16. WAIS Divide Project Members (2015) Precise interpolar phasing of abrupt climate change during the last ice age. *Nature* 520:661–665.
17. Kavanaugh JL, Cuffey KM (2003) Space and time variation of $\delta^{18}O$ and δD in Antarctic precipitation revisited. *Global Biogeochem Cy* 17(1017):1–14.
18. Sowers T, Bender M, Raynaud D, Korotkevich Y (1992) δ^{15}N of N_2 in air trapped in polar ice: A tracer of gas transport in the firn and a possible constraint on ice age-gas age differences. *J Geophys Res* 97(D14):15683–15697.
19. Severinghaus JP, Grachev A, Battle M (2001) Thermal fractionation of air in polar firn by seasonal temperature gradients. *Geochem Geophys Geosyst* 2(7):2000GC000146.
20. Herron M, Langway C (1980) Firn densification: An empirical model. *J Glaciol* 25: 373–385.
21. Goujon C, Barnola J-M, Ritz C (2003) Modeling the densification of polar firn including heat diffusion: Application to close-off characteristics and gas isotopic fractionation for Antarctica and Greenland sites. *J Geophys Res* 108(D24): 4792.
22. Schneider DP, Steig EJ, Van Ommen T (2005) High-resolution ice-core stable-isotopic records from Antarctica: Towards interannual climate reconstruction. *Ann Glaciol* 41:63–70.
23. Jouzel J, et al. (2003) Magnitude of isotope/temperature scaling for interpretation of central Antarctic ice cores. *J Geophys Res* 108(D12):4361.
24. Steig EJ, et al. (2013) Recent climate and ice-sheet changes in West Antarctica compared with the past 2,000 years. *Nat Geosci* 6:372–375.

25. Zwally HJ, Giovinetto M, Craven M, Morgan V, Goodwin I (1998) Areal distribution of the oxygen-isotope ratio in Antarctica: Comparison of results based on field and remotely sensed data. *Ann Glaciol* 27:583–590.
26. Parrenin F, et al. (2013) Synchronous change of atmospheric CO_2 and Antarctic temperature during the last deglacial warming. *Science* 339:1060–1063.
27. Nicolas JP, Bromwich DH (2011) Climate of West Antarctica and influence of marine air intrusions. *J Clim* 24:49–67.
28. Buizert C, et al. (2014) Greenland temperature response to climate forcing during the last deglaciation. *Science* 345:1177–1180.
29. Pollard D, DeConto RM (2009) Modelling West Antarctic ice sheet growth and collapse through the past five million years. *Nature* 458:329–332.
30. Golledge NR, Fogwill CJ, Mackintosh AN, Buckley KM (2012) Dynamics of the last glacial maximum Antarctic ice-sheet and its response to ocean forcing. *Proc Nat Acad Sci USA* 109:16052–16056.
31. DeConto RM, Pollard D (2016) Contribution of Antarctica to past and future sea-level rise. *Nature* 531:591–597.
32. Walsh JE (2014) Intensified warming of the arctic: Causes and impacts on middle latitudes. *Global Planet Change* 117:52–63.
33. Putnam AE, et al. (2013) Warming and glacier recession in the Rakaia valley, Southern Alps of New Zealand, during Heinrich Stadial 1. *Earth Planet Sci Lett* 382: 98–110.
34. Marcott SA, Shakun JD, Clark PU, Mix AC (2013) A reconstruction of regional and global temperature for the past 11,300 years. *Science* 339:1198–1201.
35. PALEOSENS Project Members (2012) Making sense of palaeoclimate sensitivity. *Nature* 491:683–691.
36. Schmittner A, et al. (2011) Climate sensitivity estimated from temperature reconstructions of the last glacial maximum. *Science* 334:1385–1388.
37. Fyke J, Eby M (2012) Comment on "climate sensitivity estimated from temperature reconstructions of the last glacial maximum.". *Science* 337:1294.
38. Hall BL, Porter CT, Denton GH, Lowell TV, Bromley GRM (2013) Extensive recession of Cordillera Darwin glaciers in southernmost South America during Heinrich stadial 1. *Quaternary Sci Rev* 62:49–55.
39. Boex J, et al. (2013) Rapid thinning of the late Pleistocene Patagonian Ice Sheet followed migration of the Southern Westerlies. *Sci Rep* 3:2118.
40. Putnam AE, et al. (2013) The last glacial maximum at 44 S documented by a 10 Be moraine chronology at Lake Ohau, Southern Alps of New Zealand. *Quaternary Sci Rev* 62:114–141.
41. Clark PU, et al. (2012) Global climate evolution during the last deglaciation. *Proc Natl Acad Sci USA* 109:E1134–E1142.
42. Kageyama M, et al. (2013) Climatic impacts of fresh water hosing under Last Glacial Maximum conditions: A multi-model study. *Clim Past* 9:935–953.
43. Timmerman A, Timm O, Stott L, Menviel L (2009) The roles of CO_2 and orbital forcing in driving Southern Hemispheric temperature variations during the last 21000 yr. *J Clim* 22:1626–1640.
44. Moreno PI, et al. (2015) Radiocarbon chronology of the last glacial maximum and its termination in northwestern Patagonia. *Quaternary Sci Rev* 122:233–249.
45. Doughty AM, et al. (2015) Mismatch of glacier extent and summer insolation in Southern Hemisphere mid-latitudes. *Geology* 43:407–410.
46. Marcott SA, et al. (2014) Centennial-scale changes in the global carbon cycle during the last deglaciation. *Nature* 514:616–619.
47. Buizert C, et al. (2015) The WAIS divide deep ice core WD2014 chronology–part 1: Methane synchronization (6831 ka bp) and the gas age–ice age difference. *Clim Past* 11:153–173.
48. Fudge TJ, et al. (2016) Variable relationship between accumulation and temperature in West Antarctica for the past 31,000 years. *Geophys Res Lett* 43(8): 3795–3803.
49. Patankar SV (1980) *Numerical Heat Transfer and Fluid Flow* (Hemisphere Publishing, Washington, DC).
50. Clow GD (2008) USGS polar temperature logging system, description and measurement uncertainties: *US Geological Survey Techniques and Methods 2–E3* (US Geological Survey, Reston, VA), p 24.
51. Clow GD (2014) Temperature data acquired from the DOI/GTN-P Deep Borehole Array on the Arctic Slope of Alaska, 1973–2013. *Earth Syst Sci Data* 6:201–218.
52. Orsi AJ, Cornuelle BD, Severinghaus JP (2012) Little Ice Age cold interval in West Antarctica: Evidence from borehole temperature at the West Antarctic Ice Sheet (WAIS) divide. *Geophys Res Lett* 39:L09710.
53. Sigl M, et al. (2016) The WAIS divide deep ice core WD2014 chronology–part 2: Annual-layer counting (0–31 ka bp). *Clim Past* 12:769–786.
54. Barnola J-M, Pimienta P, Raynaud D, Korotkevich YS (1991) CO_2-climate relationship as deduced from the Vostok ice core: A re-examination based on new measurements and on a re-evaluation of the air dating. *Tellus B* 43:83–90.
55. Petrenko VV, Severinghaus JP, Brook EJ, Reeh N, Schaefer H (2006) Gas records from the West Greenland ice margin covering the last glacial termination: A horizontal ice core. *Quaternary Sci Rev* 25:865–875.
56. Severinghaus JP, Baudette R, Headly MA, Taylor K, Brook EJ (2009) Oxygen-18 of O_2 records the impact of abrupt climate change on the terrestrial biosphere. *Science* 324:1431–1434.
57. Yen Y (1981) Review of thermal properties of snow, ice and sea ice. (US Army Corps of Engineers, Cold Regions Research and Engineering Laboratory, Hanover, NH), Tech Rep CR 81–10, p 34.
58. Waite WF, Gilbert LY, Winters WJ, Mason DH (2006) Estimating thermal diffusivity and specific heat from needle probe thermal conductivity data. *Rev Sci Instrum* 77(4):044904.
59. Pollard D, Chang W, Haran M, Applegate P, DeConto R (2015) Large ensemble modeling of last deglacial retreat of the West Antarctic Ice Sheet: Comparison of simple and advanced statistical techniques. *Geosci Model Devel Disc* 8:9925–9963.
60. Golledge NR, et al. (2014) Antarctic contribution to meltwater pulse 1A from reduced Southern Ocean overturning. *Nat Commun* 5:5107.
61. Steig EJ, et al. (2009) Warming of the Antarctic ice-sheet surface since the 1957 International Geophysical Year. *Nature* 457:459–462.
62. Price SF, Waddington ED, Conway H (2007) A full-stress, thermomechanical flow band model using the finite volume method. *J Geophys Res* 112:F03020.
63. Koutnik MR, et al. (2016) Holocene accumulation and ice flow near the West Antarctic Ice Sheet Divide ice core site. *J Geophys Res* 121:907–924.
64. Steig EJ, et al. (2001) West Antarctic ice sheet elevation changes. *Antarct Res* 77: 75–90.
65. Conway H, Hall BL, Denton GH, Gades AM, Waddington ED (1999) Past and future grounding-line retreat of the West Antarctic ice sheet. *Science* 286:280–283.
66. Ackert RP, Jr, et al. (1999) Measurements of past ice sheet elevations in interior West Antarctica. *Science* 286:276–280.
67. Peltier WR, Argus DF, Drummond R (2015) Space geodesy constrains ice-age terminal deglaciation: The global ICE-6G_C (VM5a) model. *J Geophys Res Solid Earth* 120 (1):450–487.
68. Resplandy L, et al. (2016) Constraints on oceanic meridional heat transport from combined measurements of oxygen and carbon. *Clim Dynam* 47(9):3335–3357.
69. Rind D, et al. (2001) Effects of glacial meltwater in the GISS coupled atmosphere-ocean model. 2. A bipolar seesaw in Atlantic Deep Water production. *J Geophys Res* 106(D21):27355–27365.
70. Barker S, et al. (2009) Interhemispheric Atlantic seesaw response during the last deglaciation. *Nature* 457:1097–1102.
71. Broccoli AJ, Dahl KA, Stouffer RJ (2006) Response of the ITCZ to Northern Hemisphere cooling. *Geophys Res Lett* 33:L01702.
72. Felzer B, Oglesby RJ, Webb T, Hyman DE (1996) Sensitivity of a general circulation model to changes in northern hemisphere ice sheets. *J Geophys Res* 101(D14): 19077–19092.
73. Zhu J, Liu Z, Zhang X, Eisenman I, Liu W (2014) Linear weakening of the AMOC in response to receding glacial ice sheets in CCSM3. *Geophys Res Lett* 41: 6252–6258.
74. Lee S-Y, Chiang JCH, Chang P (2015) Tropical Pacific response to continental ice sheet topography. *Clim Dynam* 44:2429–2446.
75. Anderson RF, et al. (2009) Wind-driven upwelling in the Southern Ocean and the deglacial rise in atmospheric CO_2. *Science* 323:1443–1448.